International Journal of Heat and Mass Transfer 189 (2022) 122693

Contents lists available at ScienceDirect

International Journal of Heat and Mass Transfer

journal homepage: www.elsevier.com/locate/hmt

Eigenfunction-based solution for solid-liquid phase change heat transfer problems with time-dependent boundary conditions

Girish Krishnan, Mohammad Parhizi, Ankur Jain*

Mechanical and Aerospace Engineering Department, University of Texas at Arlington, Arlington, TX, USA

ARTICLE INFO

Article history:
Received 22 November 2021
Revised 24 January 2022
Accepted 8 February 2022

Keywords:
Phase Change Heat Transfer
Moving Boundary Problems
Analytical Modeling
Melting
Solidification

ABSTRACT

Solid-liquid phase change heat transfer problems appear in a broad variety of engineering systems, such as thermal management and latent energy storage. Boundary conditions in such systems often vary with time, for example, due to sinusoidal heating, or step changes in externally applied temperature or heat flux. Unfortunately, phase change problems with time-dependent boundary conditions do not generally admit an exact solution, and therefore, approximate analytical solutions are of much interest. This paper presents an eigenfunction expansion based technique for solving one-dimensional phase change heat transfer problems with time-dependent temperature or heat flux boundary conditions. The temperature field is expressed as a series solution of appropriate eigenfunctions, and with time-dependent coefficients, which are determined by deriving and solving an ordinary differential equation that accounts for the time-dependent nature of the boundary condition. Solutions for Cartesian, cylindrical and spherical problems are derived. Results are found to be in excellent agreement with past work and numerical simulations. The effect of Stefan problem on the nature of phase change propagation is studied. Two practical problems involving sinusoidal and step function boundary conditions are also solved and analyzed in detail. In addition to improving the fundamental understanding of phase change heat transfer, this work may also contribute towards design and optimization of practical engineering problems involving phase change heat transfer.

1. Introduction

Solid-liquid phase change heat transfer is commonly used for energy storage and thermal management. A few representative examples include renewable energy storage [1], microelectronics cooling [2] and thermal management of Li-ion batteries [3]. Phase change heat transfer also plays a key role in several engineering processes such as manufacturing [4], desalination [5] and freezing of food [6]. Equivalent mass transfer processes are also commonly encountered, such as in Li-ion cells [7] and in silicon oxidation [8]. The large latent heat of typical Phase Change Materials (PCMs) results in high-density energy storage. However, a key fundamental challenge in phase change heat transfer pertains to its inherent self-limiting nature [9], due to thermal impedance offered by the newly formed phase, which grows over time and severely slows down further phase change. In addition, engineering challenges also exist, such as poor thermal conductivity of typical PCMs, for which, mitigation techniques such as the use of fins [10] and nano/microparticles in the PCM [11] have been proposed.

Theoretical analysis of phase change heat transfer is a well-developed research field [12,13], with the earliest theoretical models being more than a century old [14,15]. While convective heat transfer in the liquid phase and temperature-dependent properties are, in general, important, under specific conditions, such as small Grashof number [9], these may be assumed to be negligible, resulting in a simplified, pure-conduction analysis. Analytical solutions for one-dimensional phase change with constant temperature boundary condition based on self-similarity are well known [9,12]. Unfortunately, most other phase change problems do not admit an exact solution, unless the problem follows specific requirements [16–18].

In light of the lack of exact analytical solutions for several moving boundary problems that occur in phase change heat transfer, much research has been reported on the development of approximate methods, such as quasi-stationary [19], perturbation [20,21], eigenfunction expansion [22] and heat integral [23] methods. In general, such methods exhibit good accuracy when the Stefan number [9,24] is small. In addition, a number of numerical techniques are also available, such as the front fixing method [25] and the enthalpy method [26], in both mesh-based [25] and mesh-free forms [27]. Numerical techniques offer the capability to model ad-

* Corresponding author at: 500 W First St, Rm 211, Arlington, TX, USA 76019.
E-mail address: jaina@uta.edu (A. Jain).

https://doi.org/10.1016/j.ijheatmasstransfer.2022.122693
0017-9310/

Nomenclature

c_p	heat capacity ($J{\cdot}kg^{-1}{\cdot}K^{-1}$)
$\mathcal{L}$	latent heat of phase change ($J{\cdot}kg^{-1}$)
k	thermal conductivity ($W{\cdot}m^{-1}{\cdot}K^{-1}$)
b	reference length scale (m)
R_0	inner radius of hollow cylinder/sphere (m)
Ste	Stefan number, $Ste = c_p(T_{ref} - T_m)/L$
T	temperature (K)
q	heat flux ($W{\cdot}m^{-2}$)
x	spatial coordinate in Cartesian co-ordinate system (m)
r	spatial coordinate in cylindrical and spherical co-ordinate systems (m)
t	time (s)
α	diffusivity ($m^2{\cdot}s^{-1}$)
ρ	density ($kg{\cdot}m^{-3}$)
τ	non-dimensional time, $\tau = \frac{\alpha t}{b^2}$
θ	non-dimensional liquid temperature, $\theta = \frac{T_L - T_m}{T_{ref} - T_m}$
φ	non-dimensional solid temperature, $\varphi = \frac{T_S - T_m}{T_{ref} - T_m}$
Q	non-dimensional heat flux, $Q = \frac{qb}{k(T_{ref} - T_m)}$
ξ	non-dimensional spatial coordinate, $\xi = \frac{x}{b}$ (Cartesian); $\xi = \frac{r}{R_0}$ (cylindrical/ spherical)
$\lambda,\ \varepsilon,\ \eta$	non-dimensional eigenvalue in Cartesian, cylindrical and spherical problems, respectively.

Subscripts

LS	phase change front
L	liquid phase
S	solid phase
m	phase change
ref	reference
0	imposed time-dependent boundary condition

ditional complexities, such as coupled fluid flow and heat transfer [28,29], thermomechanical coupling, non-isothermal phase change [30] and complex geometries [27]. Regardless, analytical and semi-analytical solutions may still be preferred for the theoretical insight offered and ease of computation without the need for specialized simulation software.

An important class of phase change heat transfer problems among those that do not admit an analytical solution is one with time-dependent boundary conditions. Such problems occur commonly in energy storage and thermal management applications. For example, in thermal management of Li-ion cells using phase change materials [3], temperature on the cell surface, which drives the melting process in the PCM, is inherently time-dependent, due to transient conduction [31] and heat generation [32] in the cell. Similarly, heat transfer in a phase change based latent energy storage system is also highly transient [33], and therefore, requires analysis with time-dependent boundary conditions. Such problems have been solved in the past using perturbation method, in which, the solution is written in the form of a power series expansion using the Stefan number [20,21]. However, perturbation analysis can be mathematically complicated, and computation of more than the first 2-3 terms is mathematically difficult and cumbersome. It is desirable to develop an eigenfunction expansion based solution for this problem, because in this case, the accuracy of the solution can be easily tuned by considering an appropriate number of terms in the series solution. In addition, consideration of additional terms is relatively straightforward, because, unlike perturbation technique, it requires only computation of additional eigenvalues, and no new mathematical derivations. The eigenfunction expansion method models the temperature distribution in the newly formed phase as a transient conduction problem, and derives an eigenfunction-based series solution. Phase change propagation as a function of time is then determined by using the temperature distribution in interfacial energy balance at the phase change location. While this is not an exact solution, its accuracy has been shown to compare favorably with other approximate analytical methods for specific problems [22]. The eigenfunction expansion method has been used for solving phase change problems with advection [22], and with internal heat generation [34] but not for problems with time-dependent boundary conditions, such as those of interest in the present work.

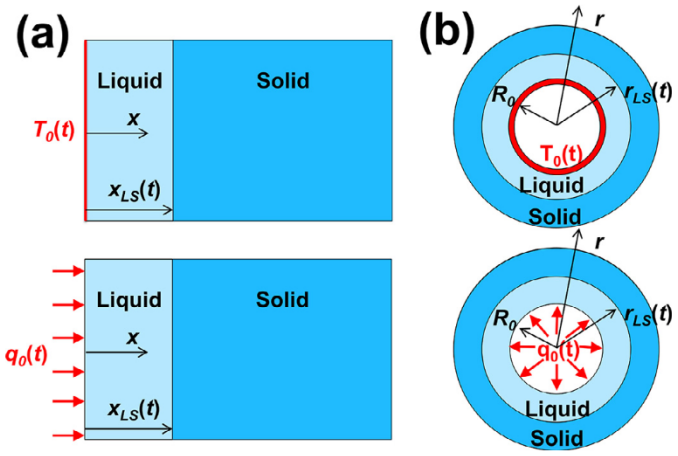

Fig. 1. Schematic of the one-dimensional phase change problem in Cartesian, Cylindrical, and Spherical co-ordinate systems with time-dependent boundary conditions. The schematic shows the melting process.

Given the practical importance of such problems, this work derives an eigenfunction expansion based solution for one-dimensional phase change problems with a time-dependent temperature or heat flux boundary condition. Solutions are derived for Cartesian, cylindrical and spherical bodies. In each case, expressions for the temperature distribution – and hence the phase change propagation as a function of time – are derived using time-dependent coefficients. Using the method of undetermined parameters [35], closed-form expressions for these coefficients are derived for each case. Results are found to agree well with past work based on other techniques, as well as with numerical simulations. The impact of Stefan number – the key non-dimensional number appearing in this problem – on phase change propagation is investigated. The nature of phase change propagation for several representative problems is analyzed. Results presented here improve the theoretical understanding of phase change heat transfer, and may also contribute towards design and optimization of phase change in energy storage and thermal management applications.

2. Mathematical Modeling

Consider the problem of phase change propagation in a one-dimensional semi-infinite Cartesian, cylindrical or spherical solid body, driven by a time-dependent temperature $T_0(t)$ or heat flux $q_0(t)$ imposed at one end of the body. Phase change is assumed to occur at a fixed temperature T_m. The body is initially at the melting temperature. Figs. 1(a)-(c) show schematics of this problem for a Cartesian, cylindrical and spherical body, respectively. In case of the Cartesian body, the boundary condition is imposed on the left face, whereas for the cylindrical and spherical problems, the phase change process is driven by heat flow into the body at the inner boundary $r=a$ due to time-dependent temperature or heat flux boundary condition, resulting in outward propagation of

the phase change front. The location of the phase change front as a function of time is often of primary interest in such problems. Phase change propagation is assumed to be one-dimensional, along the x direction for the Cartesian system, and along the outwards radial direction for the cylindrical and spherical bodies. All properties are assumed to be independent of temperature. Heat transfer driven by convective flow is neglected, i.e., the Grashof number is assumed to be very small. These are both reasonable assumptions if the temperature range in the problem is reasonably small. Phase change is assumed to occur at a fixed temperature. While presented here in the context of melting, the same framework can be used for solidification problems as well.

The next sub-sections define and solve these phase change problems in the three coordinate systems with time-dependent boundary conditions using the eigenfunction expansion method. In each case, both time-dependent temperature boundary condition, $T_0(t)$, and time-dependent heat flux boundary condition, $q_0(t)$ are considered.

2.1. Problem 1: Cartesian slab

Since the solid slab is initially at the melting temperature, there is no heat transfer into the solid phase. Referring to Fig. 1(a), the one-dimensional transient energy equation for heat conduction through the newly formed liquid phase is given by:

$$\frac{\partial^2 T_L}{\partial x^2} = \frac{1}{\alpha_L}\frac{\partial T_L}{\partial t} \tag{1}$$

where α_L is thermal diffusivity of the liquid phase and $T_L(x,t)$ is the temperature field in the liquid phase.

Within this sub-section, two distinct problems, driven by either a time-dependent temperature or time-dependent heat flux boundary condition are considered as follows.

2.1.1. Problem 1A: Time-dependent temperature boundary condition

In this case, a time-dependent temperature is imposed on the left face, which drives the melting process. The following boundary conditions apply:

$$T_L(0,t) = T_0(t) \tag{2}$$

$$T_L(x_{LS}(t),t) = T_m \tag{3}$$

$$-k_L\left[\frac{\partial T_L}{\partial x}\right]_{x=x_{LS}(t)} = \rho_L L\frac{dx_{LS}}{dt} \tag{4}$$

Eq. (2) represents the applied time-dependent temperature boundary condition on the left face that drives the phase change process. Eq. (3) represents the temperature at the melting front. Eq. (4) represents conservation of energy at the liquid-solid interface. Note that the temperature gradient in Eq. (4) refers to the one in the liquid phase.

In order to proceed, it is helpful to carry out non-dimensionalization as follows:

$$\theta = \frac{T_L - T_m}{T_{ref} - T_m};\ \tau = \frac{\alpha_L t}{b^2};\ \xi = \frac{x}{b} \tag{5}$$

Here, T_{ref} is a reference temperature and b is a reference length. The value of the imposed temperature at the initial time, $T_0(0)$, if different from T_m, may be used as T_{ref}. In contrast, the choice of b is completely arbitrary due to the absence of any length scale in the problem.

This results in the following non-dimensional set of equations for this problem:

$$\frac{\partial^2\theta}{\partial\xi^2} = \frac{\partial\theta}{\partial\tau} \tag{6}$$

subject to

$$\theta(0,\tau) = \theta_0(\tau) \tag{7}$$

$$\theta(\xi_{LS}(\tau),\tau) = 0 \tag{8}$$

$$-\left[\frac{\partial\theta}{\partial\xi}\right]_{\xi=x_{LS}(\tau)} = \frac{1}{Ste}\frac{d\xi_{LS}}{d\tau} \tag{9}$$

where $\theta_0(\tau) = \frac{T_0(t)-T_m}{T_{ref}-T_m}$ is the non-dimensional imposed temperature, and $\xi_{LS} = \frac{x_{LS}}{b}$ is the non-dimensional phase change front location. $Ste = \frac{C_{p,L}(T_{ref}-T_m)}{\mathcal{L}}$ is the Stefan number that represents the ratio of latent and sensible heat [9].

In order to solve this problem, the temperature distribution is expressed in the form of an eigenfunction series expansion with time-dependent coefficients, which are then determined based on the specified boundary condition. The resulting temperature distribution is then used in Eq. (9) to determine the phase change propagation as a function of time. Due to the time-dependent nature of the boundary condition, the method of variation of parameters [35] is used to determine the coefficients.

To begin the solution technique, the temperature distribution is assumed to be of the following form:

$$\theta(\xi,\tau) = \sum_{n=1}^{\infty} A_n(\tau)\sin(\lambda_n\xi) \tag{10}$$

where

$$\lambda_n = \frac{n\pi}{\xi_{LS}} \quad (n = 1,2,3\ldots) \tag{11}$$

Note that the sine eigenfunctions and the eigenvalues given by Eq. (11) are chosen in order to satisfy the corresponding homogeneous problem [35]. In order to determine the coefficients appearing in Eq. (10), the equation is differentiated with respect to τ. Making use of Eq. (6), one may write:

$$\frac{\partial^2\theta}{\partial\xi^2} = \sum_{n=1}^{\infty} A_n'(\tau)\sin(\lambda_n\xi) \tag{12}$$

Where A_n' refers to differentiation with respect to time. Eq. (12) is multiplied with $\sin(\lambda_m\xi)$ and integrated with respect to ξ up to the phase change front location as shown below

$$\int_0^{\xi_{LS}} \frac{\partial^2\theta}{\partial\xi^2}\sin(\lambda_m\xi)d\xi = \int_0^{\xi_{LS}} \sum_{n=1}^{\infty} A_n'(\tau)\sin(\lambda_n\xi)\sin(\lambda_m\xi)d\xi \tag{13}$$

Use of the boundary conditions and the principle of orthogonality of eigenfunctions, followed by some mathematical simplification results in the following ordinary differential equation for $A_n(\tau)$:

$$A_n'(\tau) + \lambda_n^2 A_n(\tau) = \frac{2\lambda_n\theta_0(\tau)}{\xi_{LS}} \tag{14}$$

Based on the initial condition for the problem, the initial condition associated with Eq. (14) is simply that $A_n(0) = 0$. Therefore, a solution for Eq. (14) is given by

$$A_n(\tau) = \frac{2\lambda_n}{\xi_{LS}}\int_0^{\tau} \theta_0(\tau^*)\exp\left(-\lambda_n^2(\tau-\tau^*)\right)d\tau^* \tag{15}$$

This determines the coefficients in Eq. (10), and thus temperature distribution in the newly formed liquid phase. Finally, an equation governing the phase change propagation front may be obtained by inserting Eq. (10) into Eq. (9), resulting in

$$\frac{d\xi_{LS}}{d\tau} = -Ste\frac{\partial}{\partial\xi}\left[\sum_{n=1}^{\infty} A_n(\tau)\sin(\lambda_n\xi)\right]_{\xi=\xi_{LS}(\tau)} \tag{16}$$

Where $A_n(\tau)$ are given by Eq. (15). Eq. (16) provides an explicit expression for the rate of propagation of the phase change front at any time, and, therefore, ξ_{LS} can be easily computed as a function of time, starting from the initial conditions of $\xi_{LS} = 0$ at $\tau = 0$.

2.1.2. Problem 1B: Time-dependent heat flux boundary condition

In this case, the governing energy conservation equation is still given by Eq. (6) and boundary conditions given by Eqs. (8)-(9) also apply. The boundary condition at $\xi = 0$, given by Eq. (7) for the case considered in section 2.1.1 is replaced by the following boundary conditions to represent the imposed time-dependent heat flux

$$-\left[\frac{\partial\theta}{\partial\xi}\right]_{\xi=0} = Q_0(\tau) \tag{17}$$

where $Q_0(\tau) = \frac{q_0(t)b}{k_L(T_{ref}-T_m)}$ is the imposed non-dimensional time-dependent heat flux. Unlike the previous problem, the choice of T_{ref} here is completely arbitrary due to the absence of a temperature scale in the problem.

In order to solve this problem, the following form of the temperature distribution is assumed:

$$\theta(\xi,\tau) = \sum_{n=1}^{\infty} \hat{A}_n(\tau)\sin\left(\hat{\lambda}_n(\xi_{LS}-\xi)\right) \tag{18}$$

where the eigenvalues are given by roots of $\cos(\hat{\lambda}_n\xi_{LS}) = 0$. Similar to the previous problem, the eigenvalues and eigenfunctions used here are obtained by solving the homogeneous problem corresponding to the present problem [35].

Similar to the previous sub-section, in order to solve this problem, Eq. (18) is differentiated with respect to τ and multiplied with $\sin(\hat{\lambda}_m(\xi_{LS}-\xi))$. This is followed by integration up to the phase change front as follows

$$\int_0^{\xi_{LS}} \frac{\partial^2\theta}{\partial\xi^2}\sin\left(\hat{\lambda}_m(\xi_{LS}-\xi)\right)d\xi = \int_0^{\xi_{LS}} \sum_{n=1}^{\infty} \hat{A}'_n(\tau)\sin\left(\hat{\lambda}_n(\xi_{LS}-\xi)\right)\sin\left(\hat{\lambda}_m(\xi_{LS}-\xi)\right)d\xi \tag{19}$$

Further manipulation of Eq. (19) through the use of appropriate boundary conditions and principle of orthogonality of eigenfunctions results in the following ordinary differential equation for the coefficients $\hat{A}_n(\tau)$

$$\hat{A}'_n(\tau) + \hat{\lambda}_n^2\hat{A}_n(\tau) = \frac{2(-1)^{n-1}Q_0(\tau)}{\xi_{LS}} \tag{20}$$

Given the zero initial condition for Eq. (20), a straightforward solution for $\hat{A}_n(\tau)$ is

$$\hat{A}_n(\tau) = \int_0^{\tau} \frac{2(-1)^{n-1}Q_0(\tau^*)}{\xi_{LS}}\exp\left(-\hat{\lambda}_n^2(\tau-\tau^*)\right)d\tau^* \tag{21}$$

Substituting Eq. (18) in Eq. (9) results in the following governing equation for phase change front

$$\frac{d\xi_{LS}}{d\tau} = -Ste\frac{\partial}{\partial\xi}\left[\sum_{n=1}^{\infty}\hat{A}_n(\tau)\sin\left(\hat{\lambda}_n(\xi_{LS}-\xi)\right)\right]_{\xi=\xi_{LS}(\tau)} \tag{22}$$

This completes the derivation of the solution for the Cartesian problem with time-dependent heat flux boundary condition.

2.2. Problem 2: Cylinder

The problem of outwards phase change in a hollow, semi-infinite cylinder of inner radius R_0 driven by a time-dependent boundary condition on the inner surface is considered next. The geometry for this problem is shown in Fig. 1(b). Based on the same set of assumptions as the Cartesian problem, the energy equation for this problem can be written as

$$\frac{1}{\xi}\frac{\partial}{\partial\xi}\left(\xi\frac{\partial\theta}{\partial\xi}\right) = \frac{\partial\theta}{\partial\tau} \tag{23}$$

where the radius of cylinder, R_0 is used as the reference length scale for non-dimensionalization, i.e., $\theta = \frac{T_L-T_m}{T_{ref}-T_m}$; $\tau = \frac{\alpha_L t}{R_0^2}$; $\xi = \frac{r}{R_0}$.

Two distinct cases with time-dependent temperature and heat flux boundary conditions are considered next.

2.2.1. Problem 2A: Time-dependent temperature boundary condition

In this case, a time-dependent temperature imposed on the inner wall drives the phase change process. The boundary conditions for this problem are

$$\theta(1,\tau) = \theta_0(\tau) \tag{24}$$

$$\theta(\xi_{LS}(\tau),\tau) = 0 \tag{25}$$

$$-\left[\frac{\partial\theta}{\partial\xi}\right]_{\xi=\xi_{LS}(\tau)} = \frac{1}{Ste}\frac{d\xi_{LS}}{d\tau} \tag{26}$$

where $\xi_{LS} = \frac{r_{LS}}{R_0}$ is the non-dimensional radial location of the phase change front.

Following the same procedure as section 2.1.1, one may write the solution for this problem as

$$\theta(\xi,\tau) = \sum_{n=1}^{\infty} B_n(\tau)\left(J_0(\varepsilon_n\xi) - \frac{J_0(\varepsilon_n)}{Y_0(\varepsilon_n)}Y_0(\varepsilon_n\xi)\right) \tag{27}$$

where, based on the solution of the corresponding homogeneous problem, the eigenvalues ε_n are given by roots of

$$J_0(\varepsilon_n\xi_{LS}) - \frac{J_0(\varepsilon_n)}{Y_0(\varepsilon_n)}Y_0(\varepsilon_n\xi_{LS}) = 0 \tag{28}$$

Following the same procedure as section 2.1.1, the following ordinary differential equation may be obtained for the last remaining coefficients $B_n(\tau)$

$$B'_n(\tau) + \varepsilon_n^2 B_n(\tau) = \frac{-2\theta_0(\tau)}{N_{c,n}\pi Y_0(\varepsilon_n)} \tag{30}$$

for which, the solution is

$$B_n(\tau) = \frac{-2}{N_{c,n}\pi Y_0(\varepsilon_n)}\int_0^{\tau}\theta_0(\tau^*)\exp\left(-\varepsilon_n^2(\tau-\tau^*)\right)d\tau^* \tag{31}$$

Where the norms $N_{c,n}$ are given by

$$N_{c,n} = \int_1^{\xi_{LS}} \xi\left[J_0(\varepsilon_n\xi) - \frac{J_0(\varepsilon_n)}{Y_0(\varepsilon_n)}Y_0(\varepsilon_n\xi)\right]^2 d\xi \tag{32}$$

2.2.2. Problem 2B: Time-dependent heat flux boundary condition

Here, Eq. (24) is replaced by the following equation that represents the imposed time-dependent heat flux

$$-\left[\frac{\partial\theta}{\partial\xi}\right]_{\xi=1} = Q_0(\tau) \tag{33}$$

where, similar to section 2.1.2, $Q_0(\tau) = \frac{q_0(t)R_0}{k_L(T_{ref}-T_m)}$ is the non-dimensional heat flux.

This problem is solved by assuming the following form for the temperature distribution

$$\theta(\xi,\tau) = \sum_{n=1}^{\infty}\hat{B}_n(\tau)\left(J_0\left(\hat{\varepsilon}_n\xi\right) - \frac{J_1\left(\hat{\varepsilon}_n\right)}{Y_1\left(\hat{\varepsilon}_n\right)}Y_0(\hat{\varepsilon}_n\xi)\right) \tag{34}$$

Similar to previous sections, the eigenequation determined from the homogeneous version of the problem is as follows

$$J_0\left(\hat{\varepsilon}_n\xi_{LS}\right) - \frac{J_1\left(\hat{\varepsilon}_n\right)}{Y_1\left(\hat{\varepsilon}_n\right)}Y_0\left(\hat{\varepsilon}_n\xi_{LS}\right) = 0 \tag{35}$$

Finally, the coefficients $\hat{B}_n$ can be shown to be given by

$$\hat{B}_n(\tau) = \frac{-2}{\hat{N}_{c,n}\pi\,\hat{\varepsilon}_n Y_1\left(\hat{\varepsilon}_n\right)}\int_0^\tau Q_0(\tau^*)\exp\left(-\hat{\varepsilon}_n^2(\tau-\tau^*)\right)d\tau^* \tag{36}$$

where

$$\hat{N}_{c,n} = \int_1^{\xi_{LS}} \xi\left[J_0\left(\hat{\varepsilon}_n\xi\right) - \frac{J_1\left(\hat{\varepsilon}_n\right)}{Y_1\left(\hat{\varepsilon}_n\right)}Y_0\left(\hat{\varepsilon}_n\xi\right)\right]^2 d\xi \tag{37}$$

2.3. Problem 3: Sphere

The problem of outwards phase change in a hollow, semi-infinite sphere of inner radius R_0 driven by a time-dependent boundary condition is very similar to the cylinder problem considered in the previous section. In this case, the governing energy equation is

$$\frac{1}{\xi^2}\frac{\partial}{\partial\xi}\left(\xi^2\frac{\partial\theta}{\partial\xi}\right) = \frac{\partial\theta}{\partial\tau} \tag{38}$$

2.3.1. Problem 3A: Time-dependent temperature boundary condition

The boundary conditions for the spherical problem are similar to the cylindrical problem, and therefore, are not being listed explicitly here. A solution for the problem with time-dependent temperature boundary condition can be written in the following form

$$\theta(\xi,\tau) = \sum_{n=1}^{\infty}\frac{C_n(\tau)\sin(\eta_n(1-\xi))}{\xi\sin(\eta_n)} \tag{39}$$

where the eigenequation is

$$\sin(\eta_n(1-\xi_{LS})) = 0 \tag{40}$$

The coefficients C_n can be shown to be given by the following equation:

$$C_n(\tau) = \frac{-\eta_n}{N_{s,n}\sin(\eta_n)}\int_0^\tau \theta_0(\tau^*)\exp\left(-\eta_n^2(\tau-\tau^*)\right)d\tau^* \tag{41}$$

where

$$N_{s,n} = \int_1^{\xi_{LS}}\left[\frac{\sin(\eta_n(1-\xi))}{\sin(\eta_n)}\right]^2 d\xi \tag{42}$$

2.3.2. Problem 3B: Time-dependent heat flux boundary condition

Finally, the solution for the spherical problem with time-dependent heat flux boundary condition is given by

$$\theta = \sum_{n=1}^{\infty}\hat{C}_n(\tau)\frac{\sin\left(\hat{\eta}_n(1-\xi)\right) - \hat{\eta}_n\cos\left(\hat{\eta}_n(1-\xi)\right)}{\xi\left(\sin\left(\hat{\eta}_n\right) - \hat{\eta}_n\cos\left(\hat{\eta}_n\right)\right)} \tag{43}$$

where the eigenequation is

$$\sin\left(\hat{\eta}_n(1-\xi_{LS})\right) - \hat{\eta}_n\cos\left(\hat{\eta}_n(1-\xi_{LS})\right) = 0 \tag{44}$$

The coefficients $\hat{C}_n$ for this case are given by

$$\hat{C}_n(\tau) = \frac{-\hat{\eta}_n}{\hat{N}_{s,n}\left(\sin\left(\hat{\eta}_n\right) - \hat{\eta}_n\cos\left(\hat{\eta}_n\right)\right)} \times \int_0^\tau Q_0(\tau^*)\exp\left(-\hat{\eta}_n^2(\tau-\tau^*)\right)d\tau^* \tag{45}$$

Where

$$\hat{N}_{s,n} = \int_1^{\xi_{LS}}\left[\frac{\sin\left(\hat{\eta}_n(1-\xi)\right) - \hat{\eta}_n\cos\left(\hat{\eta}_n(1-\xi)\right)}{\left(\sin\left(\hat{\eta}_n\right) - \hat{\eta}_n\cos\left(\hat{\eta}_n\right)\right)}\right]^2 d\xi \tag{46}$$

2.4. Extension to account for non-zero initial condition (two-phase problems)

Analysis presented above assumed the solid to be initially at the melting temperature. In contrast, if the semi-infinite solid is initially at a temperature T_i that is less than T_m, then heat flow into the solid beyond the phase change front occurs, resulting in a two-phase problem, also referred to as the Neumann problem. It is quite straightforward to extend the analysis presented in Section 2 to model the Neumann problem with time-dependent boundary condition. This is illustrated for the Cartesian geometry – treatment of the other two cases proceeds along similar lines. In this case, the solid temperature distribution, $T_s(x,t)$ must be determined and heat flow into the solid must be accounted for in the interfacial energy balance. In non-dimensional form, the governing equations for the solid temperature distribution may be written as

$$\frac{\partial^2\varphi}{\partial\xi^2} = \beta\frac{\partial\varphi}{\partial\tau} \tag{47}$$

$$\varphi(\xi_{LS}(\tau),\tau) = 0 \tag{48}$$

$$\varphi(\xi\to\infty,\tau) = \varphi_i \tag{49}$$

$$\varphi(\xi,0) = \varphi_i \tag{50}$$

$$-\left[\frac{\partial\theta}{\partial\xi}\right]_{x=x_{LS}(t)} + \gamma\left[\frac{\partial\varphi}{\partial\xi}\right]_{x=x_{LS}(t)} = \frac{1}{Ste}\frac{d\xi_{LS}}{d\tau} \tag{51}$$

Where $= \frac{T_S-T_m}{T_{ref}-T_m}$; $\varphi_i = \frac{T_i-T_m}{T_{ref}-T_m}$; $\beta = \frac{\alpha_L}{\alpha_S}$ and $\gamma = \frac{k_S}{k_L}$.

Note that the equations remain unaffected by the time-dependent nature of the externally applied boundary condition at $\xi = 0$ because the boundary conditions for this problem are always given by Eqs. (7) and (17). The solution for Eq. (47) subject to boundary and initial conditions shown above is as follows [9]

$$\varphi(\xi,\tau) = \varphi_i\left[\frac{erfc\left(\frac{\xi_{LS}\sqrt{\beta}}{2\sqrt{\tau}}\right) - erfc\left(\frac{\xi\sqrt{\beta}}{2\sqrt{\tau}}\right)}{erfc\left(\frac{\xi_{LS}\sqrt{\beta}}{2\sqrt{\tau}}\right)}\right] \tag{52}$$

Therefore, an equation governing the phase change propagation front for this two-phase problem can be obtained by differentiating Eq. (52) and inserting in Eq. (51), resulting in

$$\frac{d\xi_{LS}}{d\tau} = -Ste\frac{\partial}{\partial\xi}\left[\sum_{n=1}^{\infty}A_n(\tau)\sin(\lambda_n\xi)\right]_{\xi=\xi_{LS}(\tau)} + Ste\frac{\varphi_i\gamma}{erfc\left(\frac{\xi_{LS}\sqrt{\beta}}{2\sqrt{\tau}}\right)}\frac{\sqrt{\beta}}{\sqrt{\tau\pi}}\exp\left(\frac{-\beta}{4\tau}\xi_{LS}^2\right) \tag{53}$$

A two-phase problem with an initial solid of finite length, instead of semi-infinite as discussed above, can be analyzed in similar fashion. First, the temperature distribution in the finite solid can be computed, accounting for the boundary condition at the end of the solid. Subsequently, the heat flux into the solid, based on the solid temperature gradient at the phase change front can be inserted into the interfacial energy conservation equation to compute the phase change front, similar to the treatment above. Note that the finite length of the solid does not influence the one-phase problem due to the complete lack of heat flow into the solid.

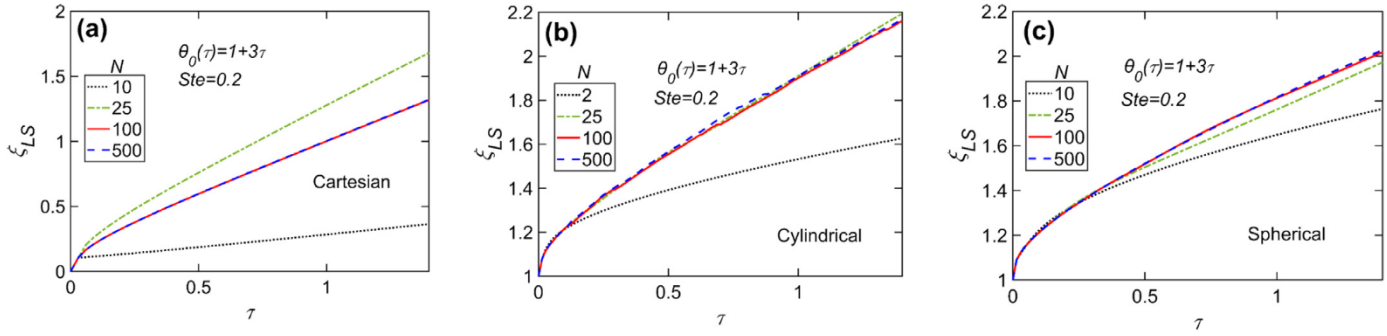

Fig. 2. Effect of the number of eigenvalues: Phase change front ξ_{LS} as a function of τ for different number of eigenvalues associated with (a) Problem 1A; (b) Problem 2A; (c) Problem 3A. The plots are presented for $\theta_0(\tau) = 1 + 3\tau$, and $Ste = 0.2$ in all the cases.

3. Results and Discussion

3.1. Effect of number of eigenvalues

Since the temperature field in this work is expressed in the form of an eigenfunction series expansion, it is important to characterize the impact of the number of eigenvalues used in the series on accuracy. Figs. 2(a), 2(b) and 2(c) present phase change front propagation curves for representative Cartesian, cylindrical and spherical problems with different number of eigenvalues. In each case, a representative expression for the imposed temperature, $\theta_0(\tau) = 1 + 3\tau$ is used. In addition, *Ste*=0.2. These curves show that around 100 eigenvalues lead to convergence in each case, with even 25 terms being reasonably sufficient for the cylindrical case. Note that while in some cases described above, the eigenvalues can be determined explicitly, in others, the eigenvalues must be computed numerically due to a lack of a closed-form solution of the eigenequation. The task of calculating eigenvalues and related coefficients is more challenging in the present problem than other similar problems, because, in the present case, the eigenvalues are a function of the phase change front, and therefore, must be re-calculated at each time as the phase change front propagates. In the present work, these eigenvalues are computed by ten successive implementations of the Newton Raphson method in regions where the eigenfunction curve is found to cross the *x*-axis. Doing so is found to result in highly accurate computation of the eigenvalues with error tolerances lower than 10^{-6}.

Based on results presented in Fig. 2, 100 eigenvalues are used for all further results presented in this section.

3.2. Comparison with past work and numerical simulations

In order to validate the present work, it is helpful to compare results from the present work with past papers that solved similar problems using other analytical techniques. Comparison for problems with specified time-dependent temperature boundary condition (problems 1A, 2A and 3A) are discussed first. Caldwell & Kwan [20] have presented analysis of a one-dimensional phase change problem with time-dependent temperature boundary condition for Cartesian, cylindrical and spherical geometries using perturbation analysis, which is an approximate technique. Comparison of results from the present work with Caldwell & Kwan is presented in Figs. 3(a)-(c) for the three geometries. Consistent with Caldwell & Kwan, expressions for time-dependent temperature boundary conditions are taken to be $\theta_0(\tau) = 1 - 0.2\tau$ for the Cartesian case (Fig. 3(a)) and $\theta_0(\tau) = 1 + \tau^2$ for the cylindrical and spherical cases (Figs. 3(b) and 3(c)). Fig. 3 shows excellent agreement for each of the three geometries considered, with a maximum deviation of only 2.6%, 2.4% and 1.6%, respectively. In Fig. 3(a), it can be observed that the phase change front starts to propagate rapidly, and slows down at larger times, as a result of reduction in the temperature boundary condition over time. In contrast, in Figs. 3(b) and 3(c), the phase change front propagates steadily because of increasing temperature at the boundary, based on the expression for $\theta_0(\tau)$. At very large times, the behavior of the curve depends on the balance between the increasing magnitude of the imposed temperature on one hand, and the increasing resistance to heat flux due to the newly formed phase on the other. A similar comparison with past work for the time-dependent heat flux case is presented in Fig. 4. For this comparison, results from Parhizi & Jain [21] are used, who also used perturbation analysis to determine an approximate solution for the Cartesian problem with a specified, time-dependent heat flux. Results for cases with linear heat flux, $Q_0(\tau) = 5000 + D\tau$, and periodic heat flux, $Q_0(\tau) = 5000(1 + \cos(\omega\tau))$ are presented for different values of D and ω in Figs. 4(a) and 4(b), respectively. Here, D and ω represent the slope and frequency of the respective heat flux profiles. Consistent with Parhizi & Jain, the value of Stefan number is taken to be $Ste = 0.008$.

Figs. 4(a) and 4(b) show very good agreement for a number of slopes and frequencies between the present work and Parhizi & Jain [21]. As the slope increases in Fig. 4(a), so does the rate of phase change front propagation. For negative values of D, the curves in Fig. 4(a) show a slowdown in phase change propagation, which is due to the reduced heat flux entering the body. As the frequency increases in Fig. 4(b), the number of oscillations in the phase change curve also increases, as expected. As expected, within the time period of interest, the propagation rate is the highest for the lowest frequency considered. There is some disagreement between the present work and Parhizi & Jain [21] at large times for low frequencies, but it is limited to around 6.3%.

Key sources of error in the present technique include the finite number of terms computed for the eigenfunction-based series solution, discretization of the phase change front equation, and the assumption of the phase change front location at the initial time step in order to kickstart the solution. The impact of these errors is minimized by taking a sufficiently large number of eigenvalues and a sufficiently small time step, so that further refinement does not significantly change the results. In contrast, perturbation method based solutions [20,21], such as the ones with which results are compared, consider only a few terms, due to the mathematical complexity involved in deriving further terms. In addition, perturbation method based solutions do not perform well at large *Ste* [20,21], whereas the techniques discussed here may have better performance. The technique discussed here is stable at large times, whereas perturbation-based and other techniques are known to diverge at large times [21]. The eigenvalues needed for the present work are quite straightforward to compute, and therefore, the present work is not computationally expensive.

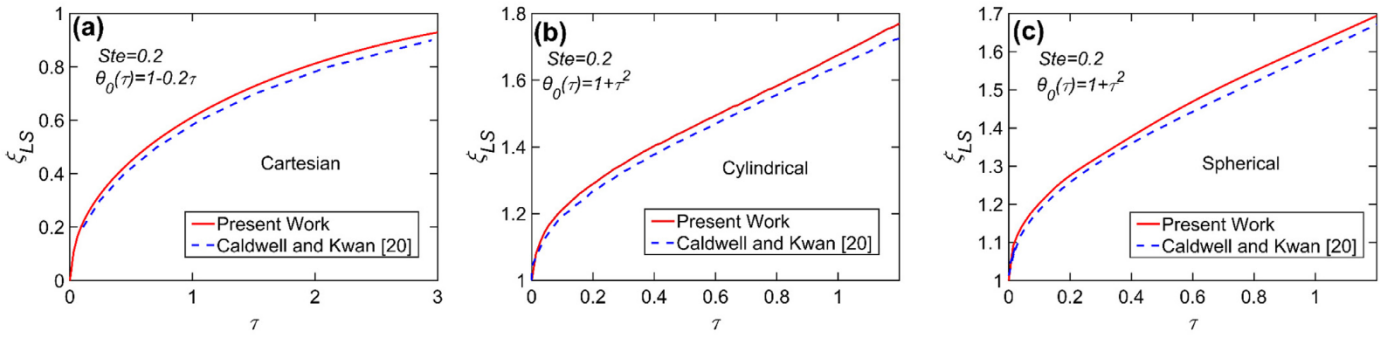

Fig. 3. Comparison of present work with past work [20] based on phase change front propagation for (a) Problem 1A with $\theta_0(\tau) = 1 - 0.2\tau$; (b) Problem 2A with $\theta_0(\tau) = 1 + \tau^2$; (c) Problem 3A with $\theta_0(\tau) = 1 + \tau^2$. The plots are presented for $Ste = 0.2$ in all the cases.

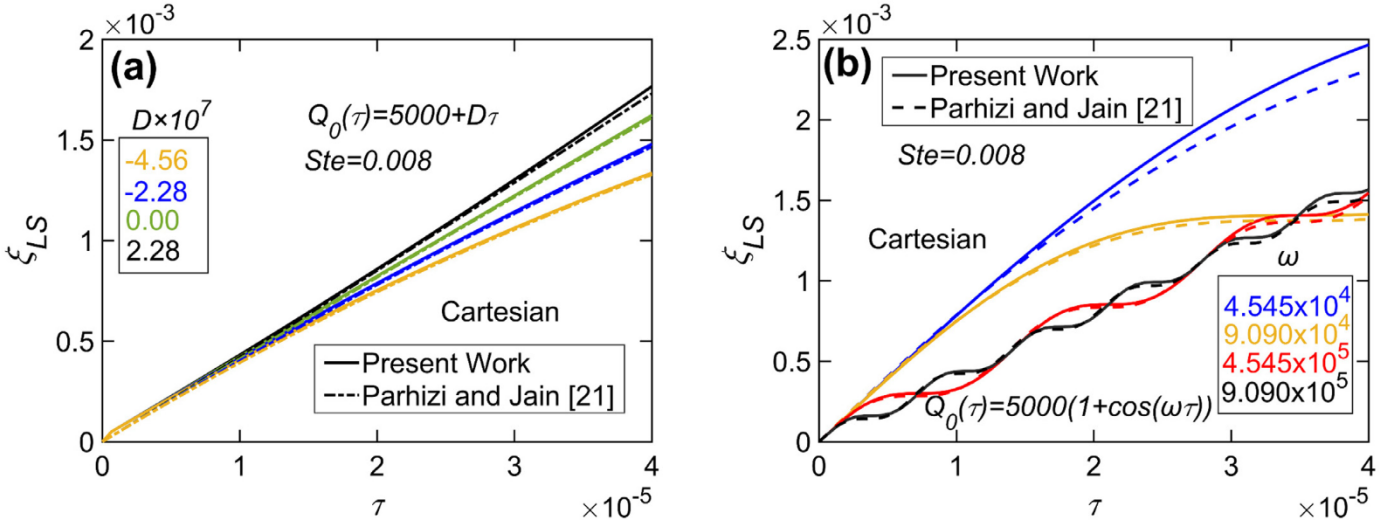

Fig. 4. Comparison of present work with past work [21] based on phase change front propagation for (a) Problem 1B with $Q_0(\tau) = 5000 + D\tau$, and $Ste = 0.008$; (b) Problem 1B with $Q_0(\tau) = 5000(1 + Cos(\omega\tau))$, and $Ste = 0.008$. The plots are presented for multiple values of D, and ω.

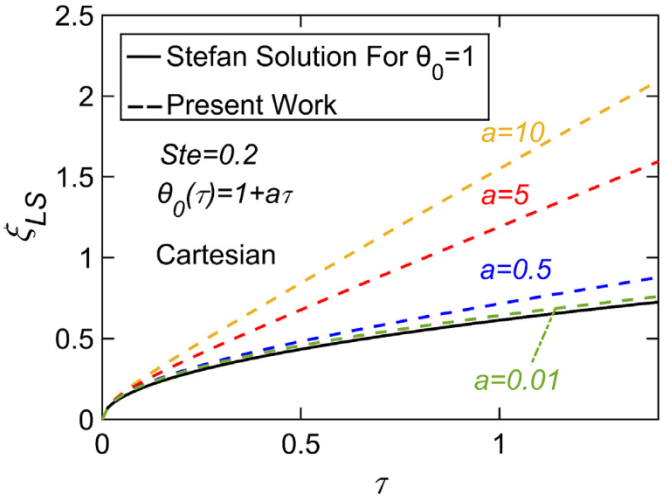

Fig. 5. Investigation of linear time-dependent boundary condition $\theta_0(\tau) = 1 + a\tau$ of Problem 1A using multiple values of a, and $Ste = 0.2$.

The case of linear time-dependent temperature boundary conditions is investigated further. For the Cartesian problem, Fig. 5 plots phase change propagation curves for $\theta_0(\tau) = 1 + a\tau$ for different values of a. The value of Stefan number is 0.2. Note that a=0 reduces this to a constant temperature boundary condition Stefan problem, for which an exact analytical solution is given by [9] $\xi_{LS} = 2\psi\sqrt{\alpha\tau}$, where ψ is the root of

$$\psi \operatorname{erf}(\psi) e^{\psi^2} = \frac{Ste}{\sqrt{\pi}} \tag{54}$$

Fig. 5 shows that as a increases, the rate of phase change propagation increases. This is along expected lines, since a large value of a results in increasing boundary temperature with time. On the other hand, as a decreases and gets close to zero, the curves approach the curve for the Stefan solution, as expected.

Finally, the present work is also validated by comparison with numerical simulations. Fig. 6(a) presents this comparison for the Cartesian problem for two time-dependent temperature boundary conditions, $\theta_0(\tau) = 1 + 3\tau$ and $\theta_0(\tau) = 1 + 3\tau^2$. A similar comparison for two time-dependent heat flux boundary conditions, $Q_0(\tau) = 1 + 2\tau$ and $Q_0(\tau) = 1 + 2\tau^2$ is presented in Fig. 6(b). The Stefan number in both cases is 0.2. The numerical simulations used here are based on a fully implicit variable time-stepping method [36], in which, the space domain is divided into equal intervals, and the duration of each successive time interval is computed such that the phase change front propagates by a distance equal to the chosen space domain interval. The accuracy of the numerical simulation itself has been established in past work [22] by comparison with the exact analytical solution for the special case of the Stefan problem with constant temperature boundary condition. Fig. 6 shows very good agreement between numerical simulations and the present work, including at large times. At small times, the curves for linear temperature boundary condition are higher than

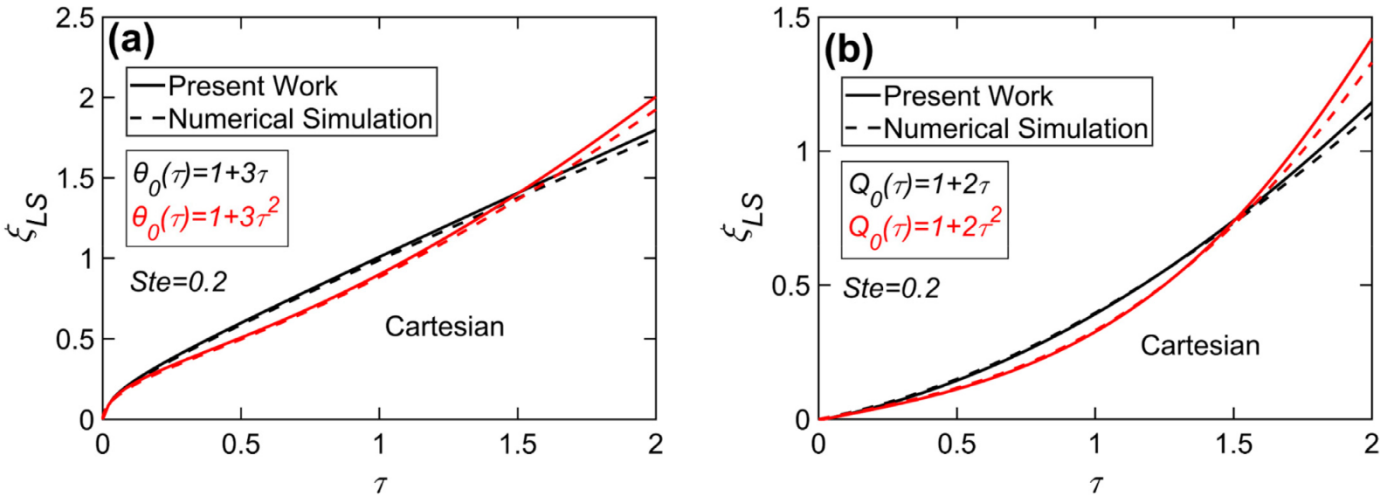

Fig. 6. Comparison of Problems 1A and 1B of present work with finite-difference numerical simulations: (a) Problem 1A with $\theta_0(\tau) = 1 + 3\tau$, and $\theta_0(\tau) = 1 + 3\tau^2$; (b) Problem 1B with $Q_0(\tau) = 1 + 2\tau$, and $Q_0(\tau) = 1 + 2\tau^2$. The plots are presented for $Ste = 0.2$ in both the cases.

the quadratic ones because, when $\tau < 1$, the linear case imposes a greater temperature on the boundary than the quadratic case. Beyond $\tau = 1$, curves for the quadratic case begin to rise faster and cross over, as the imposed temperature starts to increase rapidly.

A similar comparison of the present work with numerical simulations for cylindrical (problems 2A and 2B) and spherical (problems 3A and 3B) coordinates is presented in Supplementary Figures 1 and 2, respectively. Good agreement is observed, similar to the Cartesian case in Fig. 6.

3.3. Impact of Stefan number on phase change front propagation

The analytical model presented in Section 2 shows that Stefan number is the key non-dimensional parameter governing phase change propagation. Stefan number is the ratio between sensible heat and latent heat that, for temperature boundary condition, represents the strength of the imposed boundary condition. In case of a time-dependent temperature boundary condition, such as in Problems 1A, 2A and 3A, the Stefan number is defined on the basis of the imposed temperature at t=0. Further, for problems with heat flux boundary conditions (Problems 1B, 2B and 3B), the Stefan number is defined on the basis of a reference temperature. The impact of *Ste* on phase change propagation is examined quantitatively in Figs. 7 and 8 for the Cartesian problem. Fig. 7(a) plots the phase change front location as a function of non-dimensional time for multiple values of *Ste*. For this plot, the time-dependent temperature boundary condition at $\xi = 0$ is taken to be $\theta_0(\tau) = 1 + 3\tau$. As expected, based on the definition of the Stefan number, Fig. 7(a) shows that the rate of propagation of the phase change front increases with increasing *Ste*. Fig. 7(b) plots the phase change front location as a function of *Ste* at multiple times. As expected, the larger the value of *Ste*, the greater is the extent of phase change up to a given time. Similar plots are presented for the heat flux boundary condition problem in Figs. 8(a) and 8(b). In this case, the heat flux boundary condition is taken to be $Q_0(\tau) = 1 + 2\tau$. As before, the phase change front location increases more and more rapidly at larger values of *Ste*, and for any given time, the extent of phase change increases with *Ste*. Fig. 9 presents similar plots for phase change front propagation in a spherical body. Specifically, phase change front is plotted as a function of time for multiple values of *Ste* for time-dependent temperature ($\theta_0(\tau) = 1 + 3\tau$) and time-dependent flux ($Q_0(\tau) = 1 + \tau^2$) boundary conditions. Similar to the Cartesian plots, the extent of phase change increases with time and with the value of *Ste*.

3.4. Phase change front propagation for two common boundary conditions

Finally, Figs. 10 and 11 present results for two commonly encountered time-dependent boundary conditions. First, sinusoidal boundary condition in a Cartesian problem is investigated. A sinusoidal boundary condition is important to study because several physical phenomena inherently produce sinusoidal boundary conditions such as Joule heating due to an alternating current (AC). In addition, an arbitrary, well-behaved function can be approximated by a series of sinusoidal functions. Fig. 10(a) presents the phase change propagation plot for a time-dependent temperature boundary condition, $\theta_0(\tau) = 2(1 + \cos(\pi\omega\tau))$ for four different non-dimensional frequencies, $\omega = 1,\ 2,\ 3, 4$. Similar to Fig. 4(b), the number of oscillations in the phase change curve in Fig. 10(a) is determined by the frequency of the periodic boundary condition. At very small times, the propagation rate is invariant of the frequency, while the curves begin to distinguish at later times. After a certain time period, phase change propagation begins to slow down for each case considered here, although the $\omega = 1$ curve slows down the most, with a large period just before $\tau = 1$ where the phase change curve is nearly flat. This is indeed the period where the imposed temperature θ_0 is close to zero. Similar regions of nearly zero growth of the phase change front are seen for other values of ω, when the imposed temperature is close to zero due to the sinusoidal variation with time. Fig. 10(b) presents phase change propagation plots for cases with sinusoidal heat flux boundary condition, $Q_0(\tau) = 2(1 + \cos(\pi\omega\tau))$, for multiple values of ω. Trends similar to the temperature boundary condition plot in Fig. 10(a) are seen for this case as well.

Another interesting and commonly encountered time-dependent boundary condition is a step function, which is often used to model sudden changes in a system. For example, a step function may be used to model switching on/off of a heater element, or a sudden change in surface temperature due to external fluid flow or heat generation. Figs. 11(a) and 11(b) plot phase change front propagation as a function of time for temperature and heat flux boundary conditions defined by a step function. The boundary condition starts with a fixed value D, drops to zero at $\tau = 0.7$, and then switches back to the initial magnitude at $\tau = 1$.

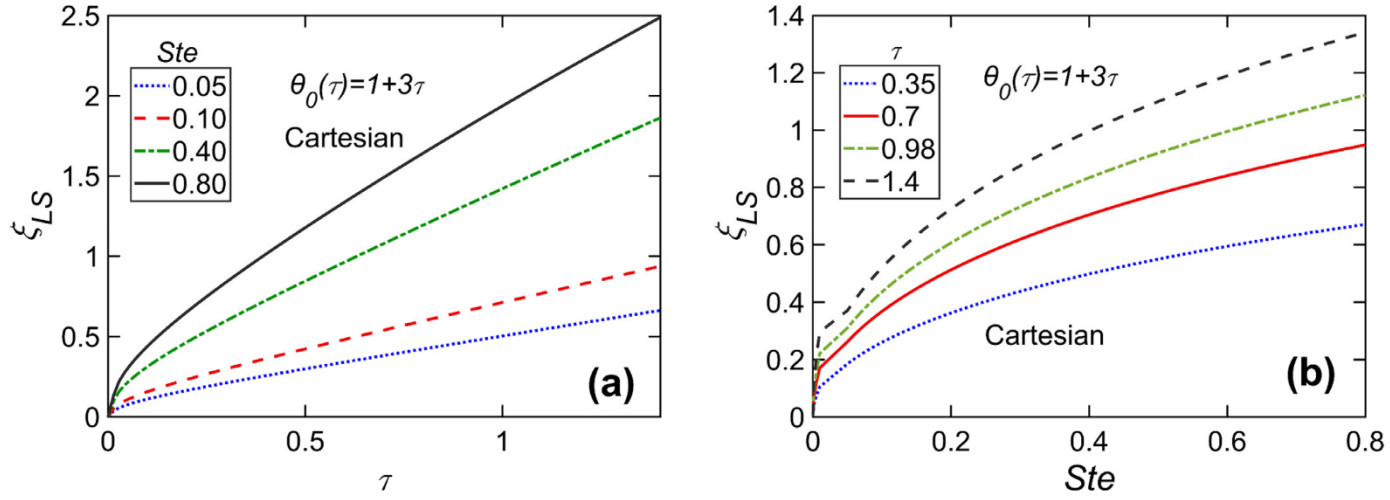

Fig. 7. Effect of *Ste* for Cartesian Problem 1A: (a) Phase change front ξ_{LS} as a function of τ for different values of *Ste*; (b) Phase change front ξ_{LS} as a function of *Ste* at different times. The boundary condition is $\theta_0(\tau) = 1 + 3\tau$.

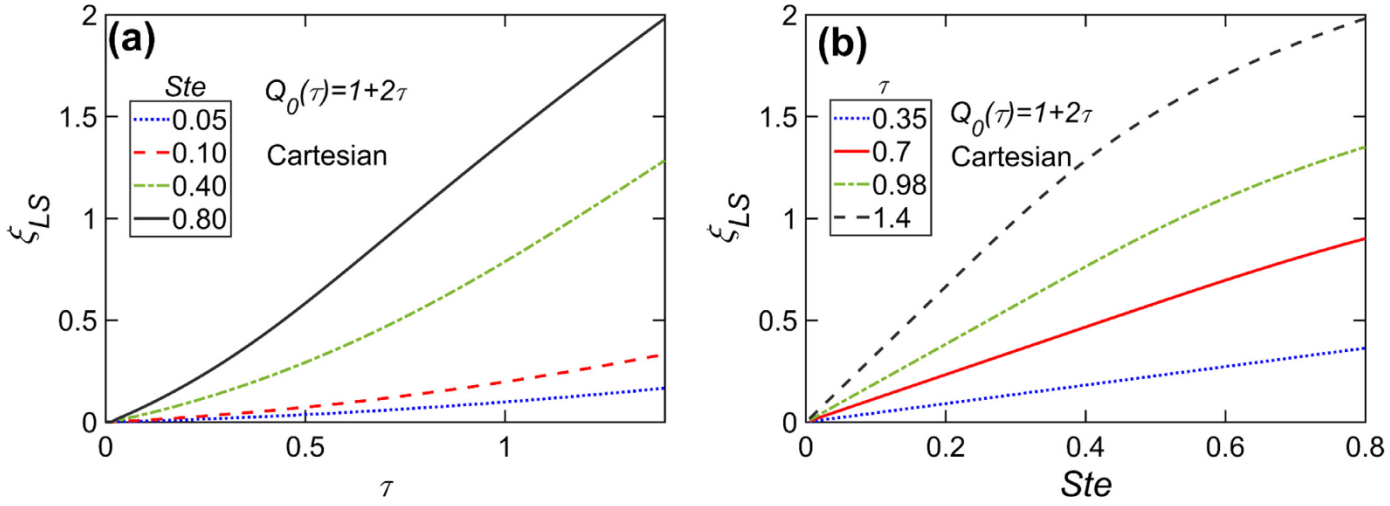

Fig. 8. Effect of *Ste* for Cartesian Problem 1B: (a) Phase change front ξ_{LS} as a function of τ for different values of *Ste*; (b) Phase change front ξ_{LS} as a function of *Ste* at different times. The boundary condition is $Q_0(\tau) = 1 + 2\tau$.

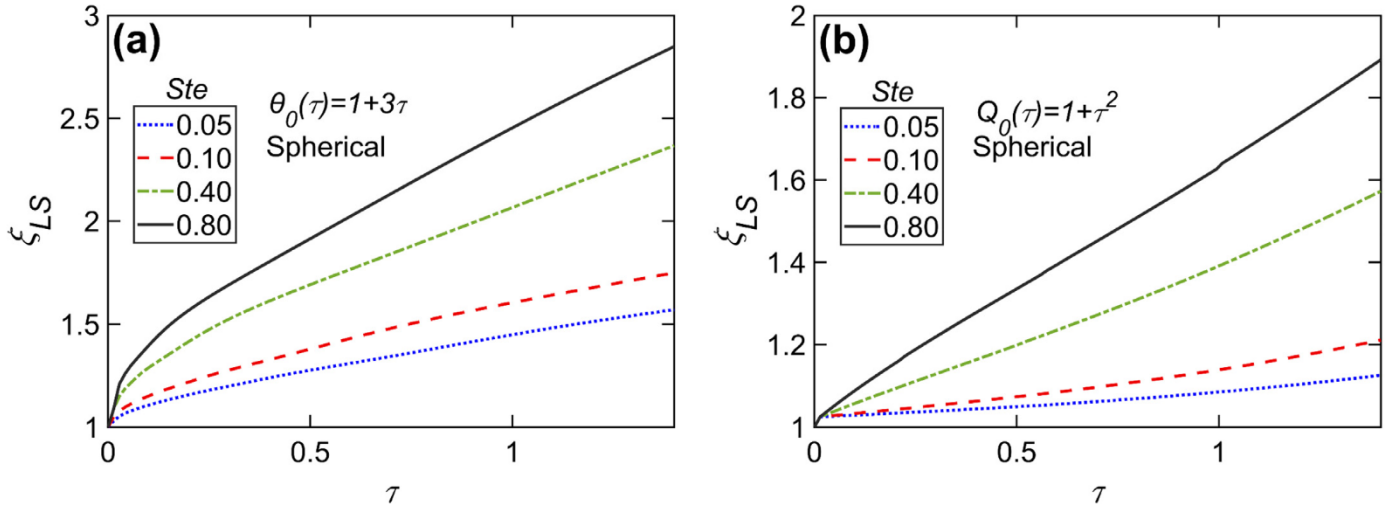

Fig. 9. Effect of *Ste* for spherical Problems 3A and 3B: (a) Phase change front ξ_{LS} as a function of τ for different values of *Ste*, and $\theta_0(\tau) = 1 + 3\tau$; (b) Phase change front ξ_{LS} as a function of τ for different values of *Ste*, and $Q_0(\tau) = 1 + \tau^2$.

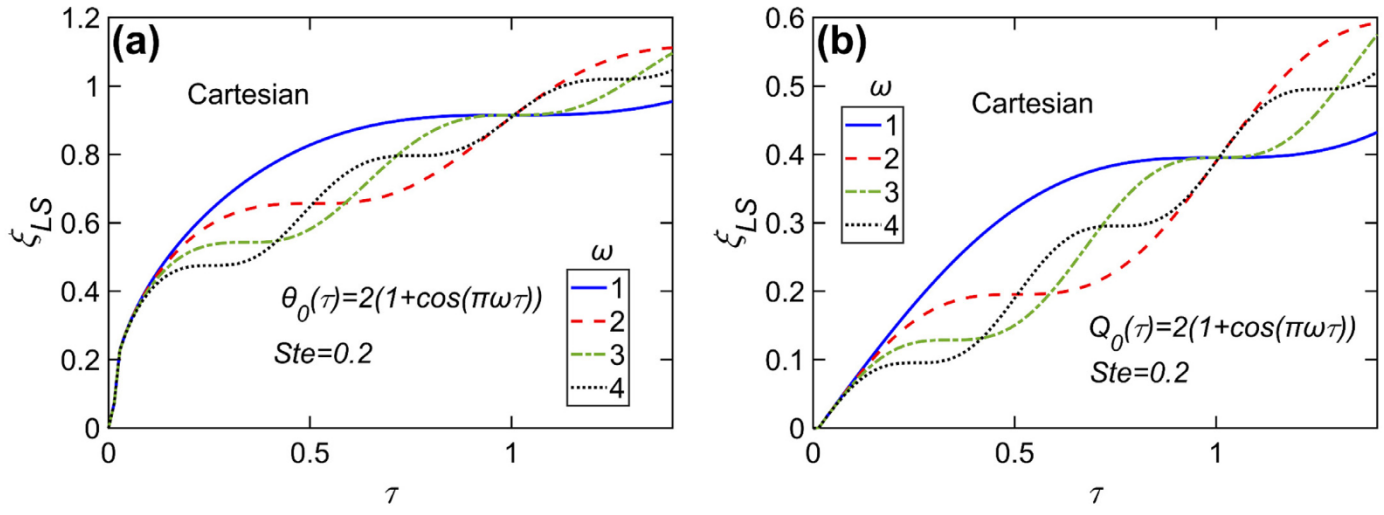

Fig. 10. Phase change front propagation for periodic time-dependent boundary conditions: (a) $\theta_0(\tau) = 2(1 + Cos(\pi\omega\tau))$; (b) $Q_0(\tau) = 2(1 + Cos(\pi\omega\tau))$. The plots are presented by solving Problems 1A and 1B for multiple values of ω, with $Ste = 0.2$.

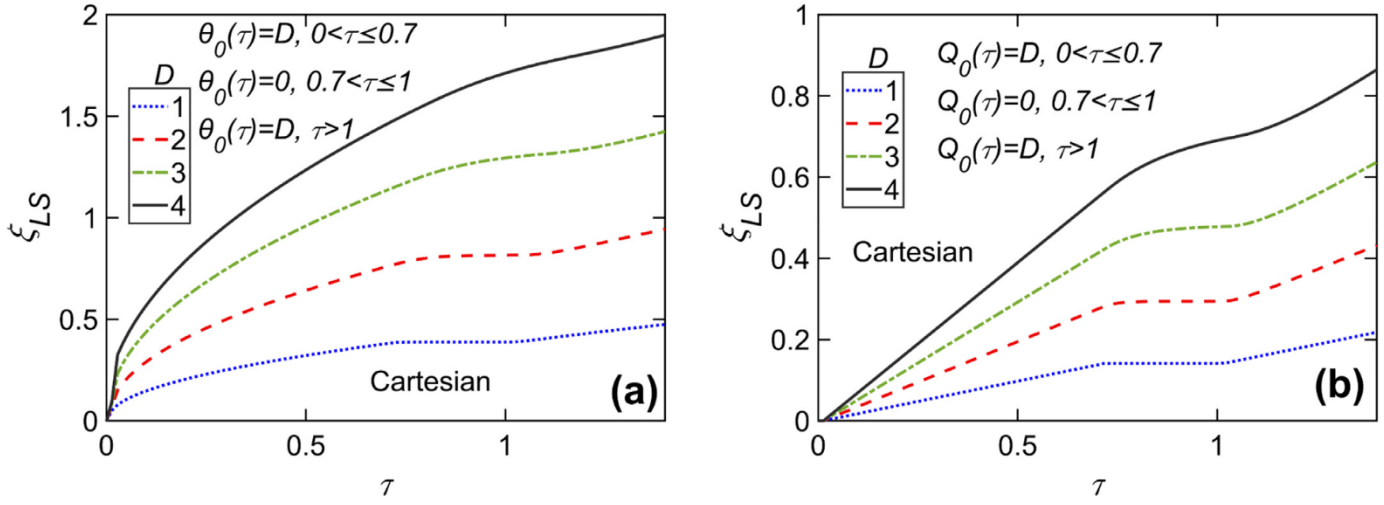

Fig. 11. Phase change front propagations for step function-based time-dependent boundary conditions: (a) $\theta_0(\tau) = D\ (0 < \tau \le 0.7)$, $\theta_0(\tau) = 0\ (0.7 < \tau \le 1)$, and $\theta_0(\tau) = D\ (\tau > 1)$; (b) $Q_0(\tau) = D\ (0 < \tau \le 0.7)$, $Q_0(\tau) = 0\ (0.7 < \tau \le 1)$, and $Q_0(\tau) = D\ (\tau > 1)$. The plots are presented by solving Problems 1A and 1B for multiple values of D. For part (a), the value of Ste is 0.1 for the $D = 1$ case. For part (b), $Ste = 0.2$.

Plots are generated for $D = 1$, 2, 3, and 4. These plots show phase change propagation as usual in the first phase, up to $\tau = 0.7$. Afterwards, when the temperature boundary condition drops down to zero, the phase change process slows down, but does not stop completely. This is because phase change continues to be driven, although at a much reduced rate, by the thermal energy available in the newly formed phase. Fig. 11(b) shows similar results for the case of a time-dependent step function heat flux boundary condition.

3.5. Results for two-phase Neumann problem

Fig. 12 plots the phase change front propagation as a function of time for a melting problem with an initially precooled solid. As discussed in Section 2.4, the solution for this problem may be obtained by a simple extension of the results presented for the case with no precooling. Assuming the same thermal properties of the liquid and solid phases, Fig. 12 plots the phase change propagation front for different precooled temperatures at Ste=0.4. As expected, the greater the degree of precooling, the slower is the phase change front propagation. This is because in the presence of a precooled solid, some of the heat that reaches the phase change

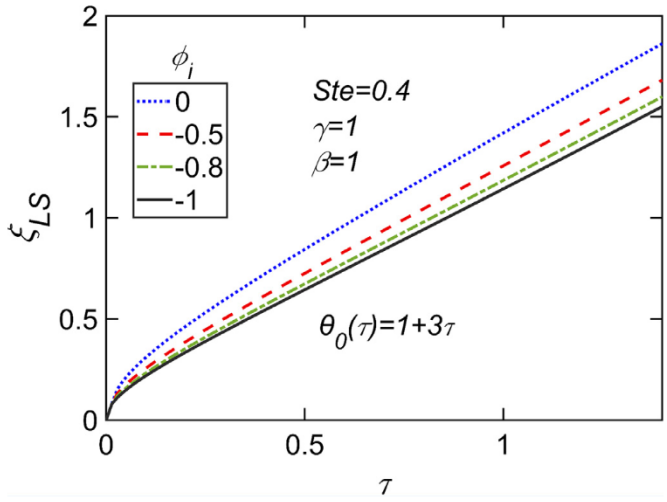

Fig. 12. Effect of solid precooling, φ_i for Cartesian Problem 1A: Phase change front ξ_{LS} as a function of τ for different values of φ_i. The boundary condition is $\theta_0(\tau) = 1 + 3\tau$.

front must diffuse into the solid rather than cause phase change. The greater the precooling, the stronger is this effect.

For the special case of a constant temperature boundary condition, Supplementary Figure 3 compares results from the two-phase problem discussed here with the analytical solution of the Neumann problem. Good agreement is observed between the two, which shows that the results from the present work for the two-phase problem correctly reduce to the Neumann solution for the case of constant temperature boundary condition, similar to the reduction of the one-phase problem to the Stefan solution, shown in Fig. 5.

5. Conclusions

Time-dependent temperature or heat flux boundary conditions appear in a broad range of practical phase change heat transfer problems. Unfortunately, such problems do not admit an exact analytical solution, which is why, the development of approximate analytical techniques is important. This paper presents eigenfunction expansion solutions of this class of problems in three key coordinate systems. Results are found to be in good agreement with past work and numerical simulations, and are found to reduce to standard results for special cases.

While the results presented here may have wide practical applications, it is also important to recognize the key limitations of the present work. Free convection in the liquid phase has been neglected, which is valid when the imposed temperature or heat flux is relatively small. Phase change is assumed to occur sharply at a fixed temperature. Further, the eigenfunction expansion technique itself is valid for small values of Stefan number. All problems are assumed to be one-dimensional, which remains a reasonable assumption for several practical problems.

Declaration of Competing Interest

All authors hereby declare that we do not have conflicts of interest as described by Elsevier's policies (http://www.elsevier.com/conflictsofinterest).

CRediT authorship contribution statement

Girish Krishnan: Methodology, Formal analysis, Investigation, Data curation, Visualization, Writing – original draft, Writing – review & editing. **Mohammad Parhizi:** Investigation, Data curation, Writing – original draft, Writing – review & editing. **Ankur Jain:** Conceptualization, Methodology, Supervision, Project administration, Data curation, Visualization, Writing – original draft, Writing – review & editing.

ACKNOWLEDGMENTS

This material is based upon work supported by CAREER Award No. CBET-1554183 from the National Science Foundation.

Supplementary materials

Supplementary material associated with this article can be found, in the online version, at doi:10.1016/j.ijheatmasstransfer.2022.122693.

References

[1] B. Zalba, J.M. Marıń, L.F. Cabeza, H. Mehling, Review on thermal energy storage with phase change: materials, heat transfer analysis and applications, Appl. Therm. Eng. 23 (2003) 251–283, doi:10.1016/S1359-4311(02)00192-8.

[2] A. Arshad, M. Jabbal, Y. Yan, Preparation and characteristics evaluation of mono and hybrid nano-enhanced phase change materials (NePCMs) for thermal management of microelectronics, Energy Conv. Management 205 (2020) 112444, doi:10.1016/j.enconman.2019.112444.

[3] M. Parhizi, A. Jain, Analytical modeling and optimization of phase change thermal management of a Li-ion battery pack, Appl. Therm. Eng. 148 (2019) 229–237, doi:10.1016/j.applthermaleng.2018.11.017.

[4] R. Viskanta, Heat transfer during melting and solidification of metals, J. Heat Transf. 110 (1988) 1205–1291, doi:10.1115/1.3250621.

[5] V.G. Gude, N. Nirmalakhandan, Desalination at low temperatures and low pressures, Desalination 244 (2009) 239–247, doi:10.1016/j.desal.2008.06.005.

[6] A. Bakal, K. Hayakawa, Heat transfer during freezing and thawing of foods, Adv. Food Res. 20 (1973) 217–256, doi:10.1016/S0065-2628(08)60195-0.

[7] M. Parhizi, M. Pathak, J. Ostanek, A. Jain, An Analytical Solution Based Iterative Model for Aging Analysis of Li-Ion Cells, J. Power Sources 517 (2022) 230667:1-12, doi:10.1016/j.jpowsour.2021.230667.

[8] B.E. Deal, A. Grove, General relationship for the thermal oxidation of silicon, J. Appl. Phys. 36 (1965) 3770–3778, doi:10.1063/1.1713945.

[9] V. Alexiades, A. D. Solomon, Mathematical Modeling of Melting and Freezing Processes, Routledge, 1993. DOI: 10.1201/9780203749449

[10] A. Mostafavi, M. Parhizi, A. Jain, Theoretical modeling and optimization of fin-based enhancement of heat transfer into a phase change material, Int. J. Heat Mass Transf. 145 (2019) 1–10 118698, doi:10.1016/j.ijheatmasstransfer.2019.118698.

[11] J.M. Khodadadi, S.F. Hosseinizadeh, Nanoparticle-enhanced phase change materials (NEPCM) with great potential for improved thermal energy storage, Int. Comm. Heat Mass Transf. 34 (2007) 534–543, doi:10.1016/j.icheatmasstransfer.2007.02.005.

[12] D.A. Tarzia, A Bibliography on Moving-free Boundary Problems for the Heat-Diffusion Equation. The Stefan and Related Problems, Instituto Matematico, Ulisse Dini", Firenze, 1988. DOI: 10.26422/MAT.A.2000.2.tar

[13] V.J. Lunardini, Heat transfer with freezing and thawing, Elsevier, 1991 ISBN: 978-0-444-88905-8.

[14] J. Stefan, Uber die Theorie des Eisbildung, insbesonder uber die Eisbildung im Polarmere, Ann. Phys. u Chem. 42 (1891) 269–286 *Neue Folge*, doi:10.1002/andp.18912780206.

[15] F. Neumann, Die partiellen Differentialgleichungen der mathematischen Physik, in: Weber Riemann (Ed.), Lectures Given in the 1860's **2**, fifth ed, 1912, p. 121.

[16] M. Turkyilmazoglu, Stefan problems for moving phase change materials and multiple solutions, Int. J. Therm. Sci. 126 (2018) 67–73, doi:10.1016/j.ijthermalsci.2017.12.019.

[17] M.F. Natale, D.A. Tarzia, Explicit solutions to the one-phase Stefan problem with temperature-dependent thermal conductivity and a convective term, Int. J. Eng. Sci. 41 (2003) 1685–1698, doi:10.1016/S0020-7225(03)00067-3.

[18] A. Jain, M. Parhizi, Conditionally Exact Closed-Form Solution for Moving Boundary Problems in Heat and Mass Transfer in the Presence of Advection, Int. J. Heat Mass Transfer 180 (2021) 1–9 121802, doi:10.1016/j.ijheatmasstransfer.2021.121802.

[19] A. Solomon, D. Wilson, V. Alexiades, The quasi-stationary approximation for the Stefan problem with a convective boundary condition, Int. J. Math. & Math. Sci. 7 (1984) 549–563, doi:10.1155/S0161171284000612.

[20] J. Caldwell, Y. Kwan, On the perturbation method for the Stefan problem with time-dependent boundary conditions, Int. J. Heat Mass Transf. 46 (2003) 1497–1501, doi:10.1016/S0017-9310(02)00415-5.

[21] M. Parhizi, A. Jain, Solution of the phase change Stefan problem with time-dependent heat flux using perturbation method, J. Heat Transfer 141 (2019) 1–5 024503, doi:10.1115/1.4041956.

[22] M. Parhizi, A. Jain, Eigenfunction-Based Solution for One-Dimensional Solid-Liquid Phase Change Heat Transfer Problems with Advection, Int. J. Therm. Sci. 172 (2022) 1–11 107262, doi:10.1016/j.ijthermalsci.2021.107262.

[23] T.R. Goodman, J.J. Shea, The Melting of Finite Slabs, J. Appl. Mech. 27 (1960) 16–24, doi:10.1115/1.3643893.

[24] A. Mori, K. Araki, Methods for analysis of moving boundary-surface problem, Int. Chem. Eng. 16 (1976) 734–744.

[25] R. Furzeland, A comparative study of numerical methods for moving boundary problems, IMA J. Appl. Math. 26 (1980) 411–429, doi:10.1093/imamat/26.4.411.

[26] V. Voller, M. Cross, Accurate solutions of moving boundary problems using the enthalpy method, Int. J. Heat Mass Transf. 24 (1981) 545–556, doi:10.1016/0017-9310(81)90062-4.

[27] E.O. Reséndiz-Flores, F.R. Saucedo-Zendjedo, Meshfree numerical simulation of free surface thermal flows in mould filling processes using the Finite Pointset Method, Int. J. Therm. Sci. 127 (2018) 29–40, doi:10.1016/j.ijthermalsci.2018.01.009.

[28] R. Guan, C. Wu, M. Zhu, Numerical modelling of fluid flow and macrosegregation in a continuous casting slab with asymmetrical bulging and mechanical reduction, Int. J. Heat Mass Transfer 141 (2019) 503–516, doi:10.1016/j.ijheatmasstransfer.2019.06.079.

[29] E.O. Reséndiz-Flores, F.R. Saucedo-Zendjedo, Numerical simulation of coupled fluid flow and heat transfer with phase change using the Finite Pointset Method, Int. J. Therm. Sci. 133 (2018) 13–21, doi:10.1016/j.ijthermalsci.2018.07.008.

[30] B. Yang, F. Bai, Y. Wang, Z. Wang, How mushy zone evolves and affects the thermal behaviours in latent heat storage and recovery: A numerical study, Int. J. Energy Research. 44 (2020) 4279–4297, doi:10.1002/er.5191.

[31] K. Shah, S. Drake, D. Wetz, J. Ostanek, S. Miller, J. Heinzel, A. Jain, An experimentally validated transient thermal model for cylindrical Li-ion cells, J. Power Sources 271 (2014) 262–268, doi:10.1016/j.jpowsour.2014.07.118.

[32] S. Drake, M. Martin, D. Wetz, J. Ostanek, S. Miller, J. Heinzel, A. Jain, Heat generation rate measurement in a Li-ion cell at large C-rates through temperature and heat flux measurements, J. Power Sources 285 (2015) 266–273, doi:10.1016/j.jpowsour.2015.03.008.
[33] A. Mostafavi, A. Jain, Analytical modeling of conjugate heat transfer between a bed of phase change material and laminar convective flow, Int. J. Heat Mass Transfer (2022) in press, doi:10.1016/j.ijheatmasstransfer.2021.122180.
[34] D. McCord, J. Crepeau, A. Siahpush, J.A.F. Brogin, Analytical solutions to the Stefan problem with internal heat generation, Appl. Therm. Eng. 103 (2016) 443–451, doi:10.1016/j.applthermaleng.2016.03.122.
[35] G.E. Myers, Analytical Methods in Conduction Heat Transfer, 2nd Ed, AMCHT Publications, Madison, WI, 1998 ISBN: 978-0966606508.
[36] D.W. Hahn, M.N. Özişik, Heat Conduction, Wiley, New York, 2012 ISBN: 978-0470902936.